




Critical behavior in the van der Waals itinerant ferromagnet Fe_4GeTe_2

Suchanda Mondal, Nazir Khan, Smruti Medha Mishra , Biswarup Satpati , and Prabhat Mandal
Saha Institute of Nuclear Physics, HBNI, 1/AF Bidhannagar, Calcutta 700 064, India

 (Received 9 April 2021; revised 13 August 2021; accepted 23 August 2021; published 2 September 2021)

The critical phenomenon of the magnetic phase transition in the van der Waals itinerant ferromagnet Fe_4GeTe_2 has been investigated by measuring the dc magnetization. The compound undergoes a continuous paramagnetic to ferromagnetic phase transition at the Curie temperature $T_C = 270.0$ K. A detailed analysis of magnetization isotherms measured in the vicinity of T_C with magnetic field H applied parallel to the ab plane yields the asymptotic critical exponents $\beta = 0.37$, $\gamma = 1.20$, and $\delta = 4.21$, whereas the magnetization isotherms for $H \parallel c$ yield $\beta = 0.34$, $\gamma = 1.20$, and $\delta = 4.52$. Both sets of the critical exponents obey the scaling relation and scaling equation of the magnetic state predicted by the scaling theory. The renormalization group theory analysis for the critical exponents and the analysis based on the self-consistent renormalization theory of spin fluctuations manifest a quasi-two-dimensional itinerant magnetism in the Fe_4GeTe_2 single crystal where the magnetic exchange coupling $J(r)$ is the long-range type that decreases spatially slower than $r^{-4.76}$. Moreover, a small reduction in the value of β for $H \parallel c$ attests to the observed weak effective uniaxial magnetic anisotropy of Fe_4GeTe_2 .

DOI: [10.1103/PhysRevB.104.094405](https://doi.org/10.1103/PhysRevB.104.094405)

I. INTRODUCTION

The quasi-two-dimensional van der Waals (vdW) bonded magnet has become a model family of materials for exploring intriguing physical properties and novel technological applications [1–5]. The coupling between the charge, spin, and lattice degrees of freedom in these low-dimensional magnets may lead to unconventional magnetoelectronic and magneto-optical properties which are elusive in the bulk. The vdW magnets in the two-dimensional (2D) limit and their heterostructures are a versatile platform for nanoelectronics and spintronic device applications [6,7]. Recently, Fe-rich vdW ferromagnets Fe_nGeTe_2 ($n \geq 3$) have received intense research interest as they appear to be promising candidates for realizing a stable material with high conductivity and large magnetization near room temperature, which are the key components for all-vdW-material-based spintronic applications [8–13]. The physical properties of these quasi-two-dimensional vdW magnets differ significantly from each other due to rather complex magnetic interaction, which is highly sensitive to their chemical composition, crystal structure, and lattice dimensionality. It has been observed that the ferromagnetic (FM) Curie temperature T_C of Fe_nGeTe_2 ranges from 200 to 363 K for $3 \leq n \leq 5$, implying Fe concentration plays a detrimental role in the magnetic exchange. Recently, in the family of Fe_nGeTe_2 , Fe_4GeTe_2 has been highlighted as a very promising candidate material for spin-source applications due to its near room temperature ferromagnetism with large magnetization, small uniaxial magnetic anisotropy, and high electrical conductivity [13].

Studying the magnetic interactions in Fe_4GeTe_2 would help in tailoring it as a spin-source material for potential technological applications and for better understanding the nature

of complex magnetic exchange mechanisms. We aim to shed some light on the nature of exchange interaction in Fe_4GeTe_2 by investigating the critical behavior of the paramagnetic (PM) to ferromagnetic phase transition. The exponents of the critical phenomenon in Fe_4GeTe_2 will reveal (i) whether the interlayer magnetic interaction is significant, (ii) the range of the spin-spin interaction, and (iii) whether the interaction is isotropic or anisotropic. In this context, the Mermin-Wagner theorem states that long-range magnetic ordering or spontaneous symmetry breaking is not possible at a nonzero temperature in the 2D limit for isotropic or Heisenberg spins [14]. Therefore, a ferromagnetic ground state of Fe_4GeTe_2 would imply that if the interlayer magnetic interaction is insignificant, then the critical exponents of Fe_4GeTe_2 are expected to be those predicted for the 2D Ising ferromagnet. If the exponents of Fe_4GeTe_2 are found to be those predicted for the three-dimensional (3D) Heisenberg ferromagnet, then the interlayer spin-spin interaction must be significant. It would also be interesting to see whether the magnetic phase transition in Fe_4GeTe_2 lies close to a tricritical point from 2D to 3D as observed in the related ferromagnet [15]. Interestingly, critical analysis of different vdW ferromagnets shows that CrSiTe_3 exhibits characteristics of a 2D Ising system, whereas CrGeTe_3 belongs to the universality class of the tricritical mean-field theory and critical exponents of CrI_3 lie between 3D Ising and the tricritical mean-field model [15–18]. Stronger interlayer magnetic interaction in CrGeTe_3 and CrI_3 compared to the others may result in this kind of magnetic critical behavior, although showing 2D structural behavior [17,18]. Similarly, a comparison of the critical phenomenon in Fe_4GeTe_2 with those of other members of the Fe_nGeTe_2 family would reveal how the stoichiometry of Fe affects the interlayer exchange interaction or the van der Waals gap and the cleavage energy.

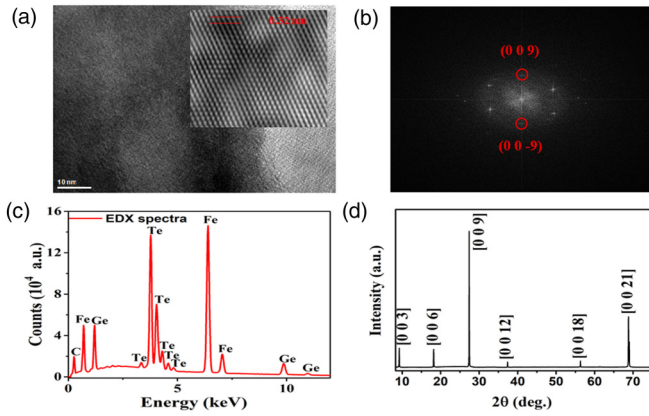


FIG. 1. (a) High-resolution transmission electron microscopy (HRTEM) image of the Fe_4GeTe_2 single crystal. (b) Fast Fourier transform pattern obtained from the HRTEM image. (c) A typical energy-dispersive x-ray (EDX) spectrum of the Fe_4GeTe_2 crystal. (d) Typical x-ray diffraction pattern obtained from the cleaved plane of the Fe_4GeTe_2 single crystal at room temperature.

II. SAMPLE PREPARATION, CHARACTERIZATION, AND METHODS

High-quality Fe_4GeTe_2 single crystals were synthesized via the standard chemical vapor transport method with iodine as the transport agent. A mixture of high-purity Fe, Ge, and Te in a molar ratio of 5:1:2 was sealed in a quartz tube under high vacuum and was heated to 725°C for 7 days (1 mol of excess Fe is essential for the formation of the Fe_4GeTe_2 phase, as discussed in an earlier work [13]). The obtained polycrystalline powdered sample was placed in an evacuated quartz tube with iodine (2 mg/cm^3) and heated for 7 days in a gradient temperature zone with one end containing the powder maintained at 800°C and the other end kept at 750°C . Small and thin single crystals with typical dimensions of $1.3 \times 1.3 \times 0.05\text{ mm}^3$ were collected from the cold end of the quartz tube. The crystals were freshly cleaved before characterization and measurements. The crystal structure analysis was carried out using a high-resolution Rigaku, TTRAX2 x-ray diffractometer with monochromatic $\text{Cu } K\alpha$ radiation. The high-resolution transmission electron microscopy (HRTEM) was done in an FEI, TECNAI G² F30, S-TWIN microscope operated at 300 kV and equipped with a GATAN Orius SC1000B CCD camera. Magnetization M was measured at ambient pressure in a superconducting quantum interference device vibrating sample magnetometer (MPMS 3, Quantum Design). For each magnetization isotherm, temperature was stabilized for more than 20 min, and data were collected at different stable magnetic fields. In Fe_4GeTe_2 , each unit cell consists of a Fe_3Ge slab with an additional Fe layer sandwiched between two Te layers which are bonded via weak vdW force with neighboring Te layers [13]. Figure 1(a) shows the HRTEM image of a typical single crystal, and it reveals the high crystalline quality of the sample over the macroscopic length scale. The value of lattice parameter c calculated from interlayer separation is 28.8 \AA , which matches well with a previous report on Fe_4GeTe_2 for hexagonal crystal structure [13]. Figure 1(b) displays the fast Fourier transform pattern obtained from the

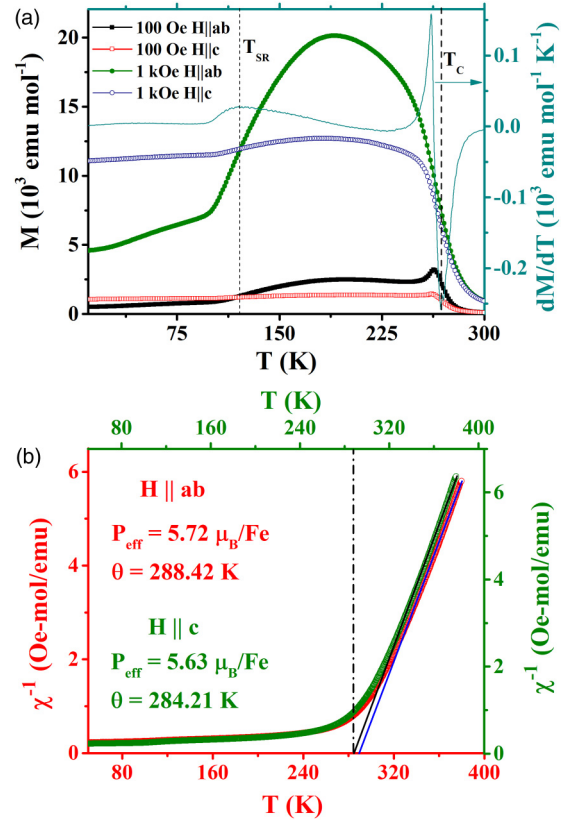


FIG. 2. (a) Temperature dependence of the dc magnetization measured in the zero-field-cooled condition for applied magnetic field $H = 0.1$ and 1 kOe with $H \parallel ab$ and $H \parallel c$. The right axis shows the first derivative of the magnetization dM/dT and suggests $T_C \sim 270\text{ K}$, where the rate of increase of magnetization is maximum as the compound enters into a magnetically ordered state. T_{SR} indicates the temperature below which a spin reorientation takes place in Fe_4GeTe_2 . (b) Temperature dependence of inverse magnetic susceptibilities for the Fe_4GeTe_2 single crystal. Fitting with the Curie-Weiss law is indicated by solid lines.

HRTEM image shown in Fig. 1(a). The Miller indices of the corresponding lattice planes are marked in the image. We have performed energy-dispersive x-ray (EDX) spectroscopy on the as-grown crystal to check the elemental composition and chemical homogeneity. The obtained result from EDX spectroscopy confirms that the Fe, Ge, and Te atomic ratio is 4.2:1:1.9 with a relative error of $\sim 5\%$, which is close to the desired stoichiometry [Fig. 1(c)]. Figure 1(d) shows the x-ray diffraction (XRD) pattern for thin single crystals of Fe_4GeTe_2 . The presence of extremely sharp and only equivalent Bragg's reflections confirms the high crystallinity of the grown single crystals with the flat surface parallel to the ab plane. The calculated lattice parameter, c , from the refinement of the XRD pattern is estimated to be 28.74 \AA , which is close to the previously reported value [13].

III. RESULTS AND DISCUSSION

Figure 2(a) shows the temperature dependence of the zero-field-cooled dc magnetization for magnetic fields $H = 0.10$ and 1 kOe , which are applied parallel to the ab plane and c

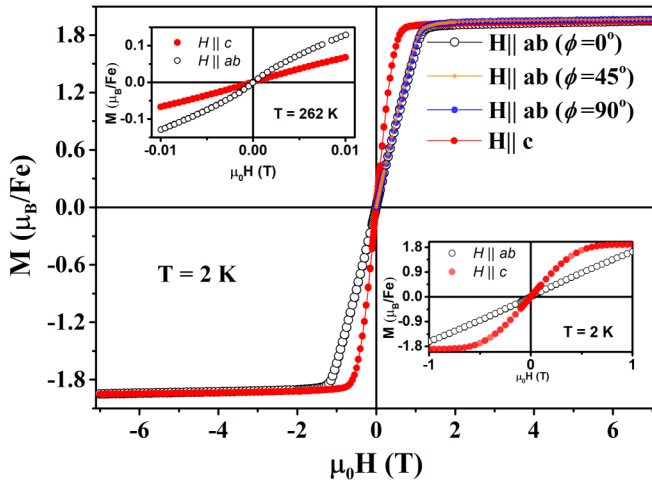


FIG. 3. Isothermal magnetization for both the $H\parallel ab$ plane and $H\parallel c$ axis at $T = 2$ K. The in-plane $M(\phi)$ was measured under the field within the ab plane displaying isotropic magnetization. Insets show the H dependence of the magnetization at $T = 2$ K (lower inset) and 262 K (upper inset) in the low-field region and illustrate that the magnetic easy axis lies in the ab plane above T_{SR} and is then rotated to the c axis at low temperatures.

axis of the Fe_4GeTe_2 single crystal. The $M(T)$ curves show that the magnetization increases upon cooling and undergoes a paramagnetic to ferromagnetic phase transition at around 270 K, where the temperature derivative of the magnetization dM/dT attains its minimum, suggesting critical temperature $T_C \sim 270$ K. Upon further cooling well below T_C , an additional feature is observed in the M vs T curve at temperature $T_{SR} \sim 120$ K. Below T_{SR} , a spin-reorientation phenomenon occurs in the Fe_4GeTe_2 compound, and as a result, the out-of-plane magnetization becomes larger than the in-plane magnetization [13]. This crossover in magnetization below the spin-reorientation transition temperature in Fe_4GeTe_2 is quite distinct from other members of the Fe_nGeTe_2 series for which the absolute value of magnetization for $H\parallel ab$ always remains larger than that for $H\parallel c$ throughout the temperature region below 300 K [19].

The temperature dependence of paramagnetic susceptibility χ may reveal important information on magnetic interaction and the spin state of the Fe ion in Fe_4GeTe_2 . Figure 2(b) shows the temperature dependence of inverse susceptibility χ^{-1} measured under a dc field of $H = 10$ kOe with applied field both parallel and perpendicular to the ab plane. It is clear from Fig. 2(b) that $\chi^{-1}(T)$ for both directions are very close to each other and linear at high temperatures. We have fitted χ^{-1} vs T data with the Curie-Weiss (CW) expression, $\chi = \frac{C}{T - \theta}$, where $C = \frac{Ng^2\mu_B^2 J(J+1)}{3k_B}$ is the Curie constant and θ is CW temperature. The fits yield effective magnetic moment $P_{\text{eff}} = 5.72 \mu_B/\text{Fe}$ with Curie temperature $\theta_{ab} = 288.42$ K for the $H\parallel ab$ direction, and the corresponding values are $5.63 \mu_B/\text{Fe}$ and 284.21 K for the $H\parallel c$ configuration. These values indicate the nearly isotropic paramagnetic behavior of the Fe_4GeTe_2 single crystal.

Figure 3 shows isothermal magnetization at $T = 2$ K measured up to a magnetic field of 7 T for both $H\parallel ab$ and

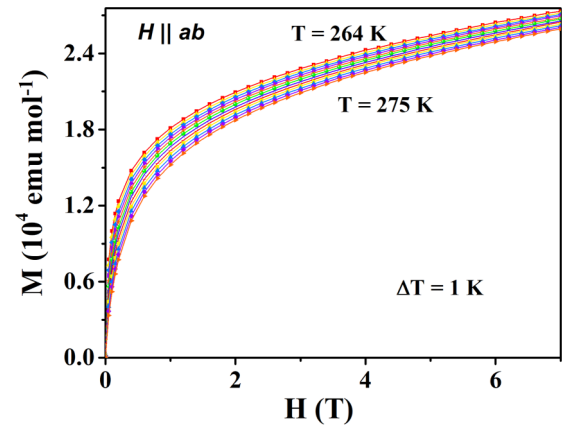


FIG. 4. Isothermal magnetization as a function of magnetic field (M vs H) at different temperatures measured around T_C for magnetic field applied parallel to the ab plane of the Fe_4GeTe_2 single crystal.

$H\parallel c$ orientations. The high-field saturation magnetization is estimated to be about $1.9\mu_B/\text{Fe}$. The insets show the magnetization isotherms at $T = 2$ and 262 K in the low-field region which demonstrate that the magnetic easy axis lies in the ab plane at high temperature above T_{SR} and then rotate toward the c axis at low temperature due to the reorientation of Fe spins. The transition temperature $T_C = 270$ K and all the features in the temperature and field dependence of the magnetization in the present Fe_4GeTe_2 single crystal are in excellent agreement with a previous study on a well-characterized Fe_4GeTe_2 single crystal [13]. Angle-dependent magnetization $M(\phi)$ is measured at 2 K for field applied along three different directions within the ab plane (Fig. 3). The magnetizations at $\phi = 0^\circ$, 45° , and 90° for $H\parallel ab$ are almost identical, which implies an isotropic nature of in-plane magnetization of the Fe_4GeTe_2 single crystal.

To investigate the critical behavior of the PM to FM phase transition in Fe_4GeTe_2 , magnetization isotherms in the temperature range $264 \leq T \leq 275$ K were measured in the close vicinity of T_C for magnetic field $H\parallel ab$ and $H\parallel c$ directions. The data for isotherms were collected with a temperature interval $\Delta T = 0.5$ K. Figure 4 shows the magnetization isotherms for magnetic field $H\parallel ab$ where only isotherms with $\Delta T = 1.0$ K are presented for better representation. For a continuous magnetic phase transition to a long-range magnetic order, the spin-spin correlation length ξ diverges at the critical temperature, leading to universal behavior of different thermodynamic quantities governed by the critical fluctuation. The critical behavior is characterized by a set of static critical exponents whose values depend only on the symmetry of the order parameter and the dimensionality of the lattice and are independent of the microscopic details of the homogeneous magnet. For the magnetic phase transition, the spontaneous magnetization $M_S(0, T)$ below T_C , the inverse initial susceptibility $\chi_0^{-1}(0, T)$ above T_C , and the magnetization isotherm $M(H, T_C)$ at T_C are characterized by a set of static critical exponents β , γ , and δ , respectively. These exponents are given by the following power laws

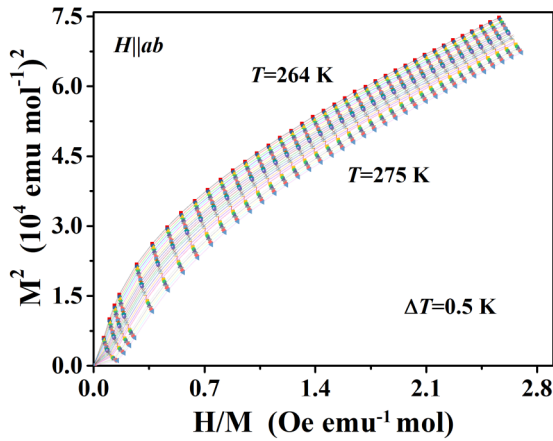


FIG. 5. Arrott plot of M^2 vs H/M isotherms in the vicinity of T_C with temperature interval $\Delta T = 0.5$ K for $H\parallel ab$.

[20]:

$$M_S(0, T) = [M_S(0)](-\varepsilon)^\beta, \quad \varepsilon < 0, \quad (1)$$

$$\chi_0^{-1}(0, T) = \left[\frac{H_0}{M_S(0)} \right] (\varepsilon)^\gamma, \quad \varepsilon > 0, \quad (2)$$

$$M(H, T_C) = D(H)^{1/\delta}, \quad \varepsilon = 0, \quad (3)$$

where $\varepsilon = \frac{T-T_C}{T_C}$ is the reduced temperature and $M_S(0)$, $\frac{H_0}{M_S(0)}$, and D are the critical amplitudes. The scaling theory of continuous phase transition predicts that in the close vicinity of the phase transition, the magnetic equation of state for the system can be written as

$$M(H, \varepsilon) = |\varepsilon|^\beta f_\pm \left[\frac{H}{|\varepsilon|^{(\gamma+\beta)}} \right], \quad (4)$$

where f_+ and f_- are regular functions for temperature above and below T_C , respectively. In terms of the scaled or renormalized magnetization, $m \equiv |\varepsilon|^{-\beta} M(H, \varepsilon)$, and the renormalized field, $h \equiv |\varepsilon|^{-(\gamma+\beta)} H$, the above magnetic equation of state can be rewritten as

$$m = f_\pm(h). \quad (5)$$

Equation (5) implies that for the correct values of β , γ , and ε , the m vs h isotherms will fall onto two separate branches of the scaling function: f_+ for isotherms above T_C and f_- for isotherms below T_C . This is also an important criterion to check whether the same set of the critical exponents can be used to describe the magnetic field dependence of magnetization both below and above T_C .

Figure 5 shows the conventional Arrott plot of M^2 vs H/M isotherms for the Fe_4GeTe_2 single crystal obtained from isotherms presented in Fig. 4 [21]. For the mean-field values of the critical exponents ($\beta = 0.5$ and $\gamma = 1$), the isotherms in the Arrott plot should constitute a set of parallel straight lines, and the isotherm at the critical temperature would pass through the origin of the plot. However, isotherms in the Arrott plot of Fe_4GeTe_2 are far from a set of parallel straight lines and show significant nonlinearity or curvature even at magnetic field up to 7 T. Therefore, the Landau mean-field theory of continuous phase transition does not hold for the Fe_4GeTe_2 compound and suggests the presence of significant

critical fluctuations in the close vicinity of T_C . Furthermore, according to Banerjee's criterion [22], the slope of the Arrott plot isotherms for a second-order phase transition is positive. In Fig. 5, all the M^2 vs H/M isotherms show concave downward curvature, leading to positive values of the slopes and thereby assert that the nature of FM to PM phase transition in Fe_4GeTe_2 is second order. The Arrott plot of magnetization isotherms for $H\parallel c$ is qualitatively similar to that for $H\parallel ab$ (not shown). However, it must be mentioned that the demagnetization effect is significant for $H\parallel c$, and therefore, in the analysis of critical behavior for $H\parallel c$ the applied magnetic field H_{app} was corrected following $H_{\text{in}} = H_{\text{app}} - 4\pi NM$, where N is the demagnetization factor, M is magnetization per unit volume, and H_{in} denotes the internal magnetic field [23]. Data for this direction of applied field have been corrected considering the calculated value of the demagnetization factor of 0.745. Since the demagnetization effect is very small for field applied parallel to the ab plane, data have been corrected for only the $H\parallel c$ direction.

In the presence of critical magnetization fluctuations, the most widely used method to determine the critical exponents β and γ is the modified Arrott plot [24] technique which is based on the following Arrott-Noaks equation of state:

$$(H/M)^{1/\gamma} = a \left(\frac{T - T_C}{T_C} \right) + bM^{1/\beta}, \quad (6)$$

where the coefficients a and b are temperature independent but their values are system dependent. Several modified Arrott plots have been constructed using different sets of β and γ values, including that predicted by theoretical models for the 3D system such as the 3D Heisenberg model ($\beta = 0.365$, $\gamma = 1.386$), the 3D XY model ($\beta = 0.345$, $\gamma = 1.316$), and the 3D Ising model ($\beta = 0.325$, $\gamma = 1.24$). The intercepts of the linear fits in the high-field region of each modified Arrott plot isotherm with axes $M^{1/\beta}$ and $(H/M)^{1/\gamma}$ yield values of $M_S(0, T)$ and $\chi_0^{-1}(0, T)$, respectively, at different temperatures. At low field, magnetic domains are not unidirectional. As a result, averaging over these domains causes a small deviation from linearity in the modified Arrott plot in the low-field region. The power-law fits to the T dependence of $M_S(0, T)$ and $\chi_0^{-1}(0, T)$ yield a new set of β and γ values, respectively, for each modified Arrott plot. The values of β and γ of the final modified Arrott plot correspond to the values which match that obtained from the power-law fits to the $M_S(0, T)$ and $\chi_0^{-1}(0, T)$ data. Figures 6(a) and 6(b) show modified Arrott plots of the Fe_4GeTe_2 single crystal for $H\parallel ab$ and $H\parallel c$, respectively. The $M_S(0, T)$ and $\chi_0^{-1}(0, T)$ curves obtained from the corresponding modified Arrott plots are shown in Figs. 7(a) and 8(a). It can be seen that the values of β and γ corresponding to the final modified Arrott plots are $\beta = 0.37$, $\gamma = 1.20$ and $\beta = 0.34$, $\gamma = 1.20$ for $H\parallel ab$ and $H\parallel c$, respectively. The values of β and γ obtained from the power-law fits to the $M_S(0, T)$ and $\chi_0^{-1}(0, T)$ data are $\beta = 0.37(1)$, $\gamma = 1.21(3)$ for $H\parallel ab$ and $\beta = 0.33(1)$, $\gamma = 1.17(4)$ for $H\parallel c$, as shown in Figs. 7(a) and 8(a), respectively. These estimated values of β and γ match quite well with that of the corresponding modified Arrott plots. Figures 6(a) and 6(b) show that the isotherms at $T = 270.0$ K of both the modified Arrott plots almost pass through the origin of the respective plots, indicating that the critical temperature of the magnetic

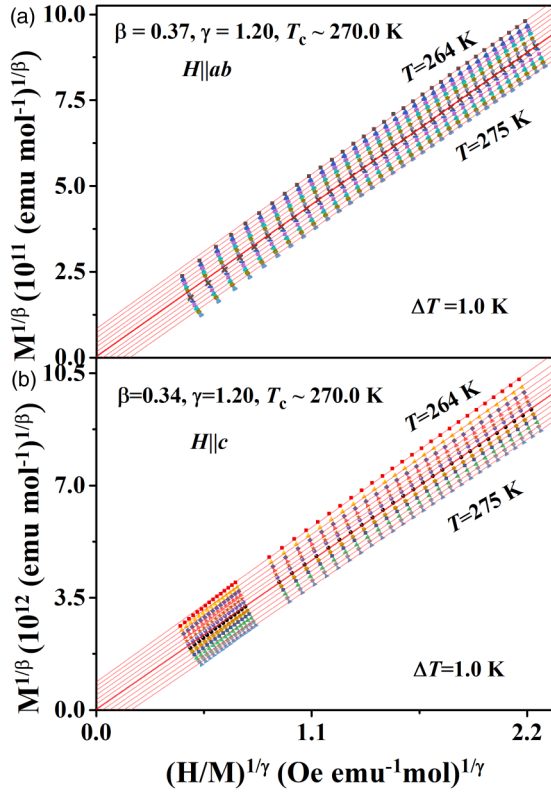


FIG. 6. Modified Arrott plots of isotherms in the temperature range $264.0 \text{ K} \leq T \leq 275.0 \text{ K}$, where (a) $\beta = 0.37$ and $\gamma = 1.20$ for the applied field $H \parallel ab$ and (b) $\beta = 0.34$ and $\gamma = 1.20$ for the applied field $H \parallel c$. Solid lines are the least-squares linear fits to the isotherms. The isotherms of $T = 270 \text{ K}$ for $H \parallel ab$ and $H \parallel c$ almost pass through the origin of the respective plot, suggesting the critical temperature $T_c = 270.0 \text{ K}$.

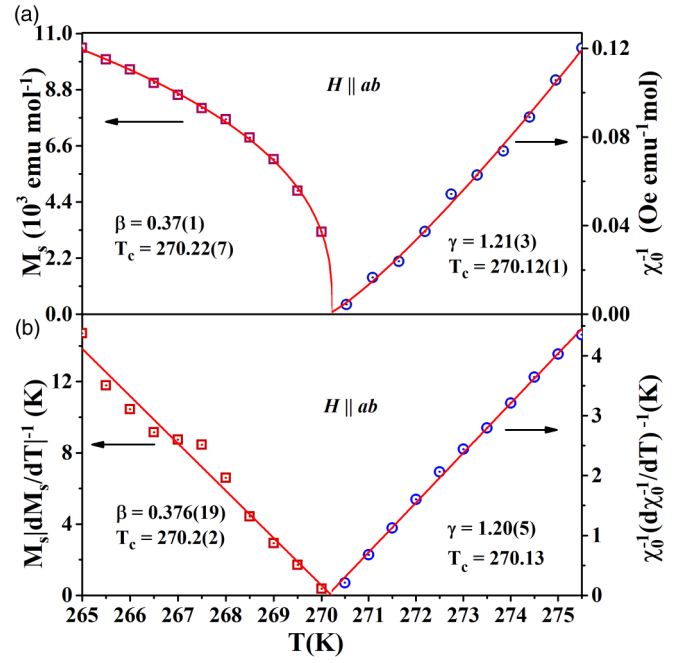


FIG. 7. (a) Temperature dependence of M_S and χ_0^{-1} for $H \parallel ab$ along with the power-law fits (solid lines) following Eqs. (1) and (2). The least-squares fitting yields the values of the exponents and T_c mentioned in the plot. (b) Kouvel-Fisher plot of M_S and χ_0^{-1} as mentioned in the text. The exponents and T_c are obtained from the linear fits (solid lines) of the data in this plot.

phase transition in Fe_4GeTe_2 is close to 270 K . The critical temperature obtained from the power-law fits to the $M_S(0, T)$ and $\chi_0^{-1}(0, T)$ curves in Figs. 7(a) and 8(a) is also very close to 270 K .

TABLE I. Comparison of the critical exponents of Fe_4GeTe_2 with earlier reports on other related van der Waals ferromagnets and different theoretical models. Abbreviations: MAP, modified Arrott plot; KF, Kouvel-Fisher; CI, critical isotherm; LR, long range; RG- ϵ' , renormalization group epsilon ($\epsilon' = 2\sigma - d$) expansion.

Material/Model	Ref.	Technique		T_c (K)	β	γ	δ
Fe_4GeTe_2	This work	MAP	$H \parallel ab$	270.2(1)	0.37(1)	1.21(3)	4.24(2)
			$H \parallel c$	270.2(1)	0.33(1)	1.17(43)	4.54(2)
	This work	KF	$H \parallel ab$	270.2(2)	0.376(19)	1.20(5)	4.22(14)
			$H \parallel c$	270.1(1)	0.33(1)	1.20(1)	4.63(1)
	This work	CI	$H \parallel ab$	270.0(2)			4.21(1)
			$H \parallel c$	270.0(1)			4.52(1)
Fe_5GeTe_2	[27]	KF		273.7	0.346(10)	1.364(9)	4.94(0)
Fe_3GeTe_2	[28]	KF		215.1	0.322(4)	1.063(8)	4.301(6)
$\text{Fe}_{3-x}\text{GeTe}_2$	[29]	KF		151.2	0.372(4)	1.265(1)	4.401(6)
Mean field	[20]	Theory			0.5	1	3
Tricritical mean field	[20]	Theory			0.25	1	5
3D Heisenberg	[22,30]	Theory			0.365	1.386	4.8
3D XY	[22,31]	Theory			0.345	1.316	4.81
3D Ising	[22,31]	Theory			0.325	1.24	4.82
LR exchange: $J(r) = 1/r^{d+\sigma}$							
$d = 3, n = 3, \sigma = 1.76$	[20,32]	RG- ϵ'			0.423	1.200	3.838
$d = 2, n = 3, \sigma = 1.17$	[20,32]	RG- ϵ'			0.426	1.201	3.819
$d = 2, n = 2, \sigma = 1.19$	[20,32]	RG- ϵ'			0.408	1.200	3.938
$d = 2, n = 1, \sigma = 1.23$	[20,32]	RG- ϵ'			0.377	1.206	4.195

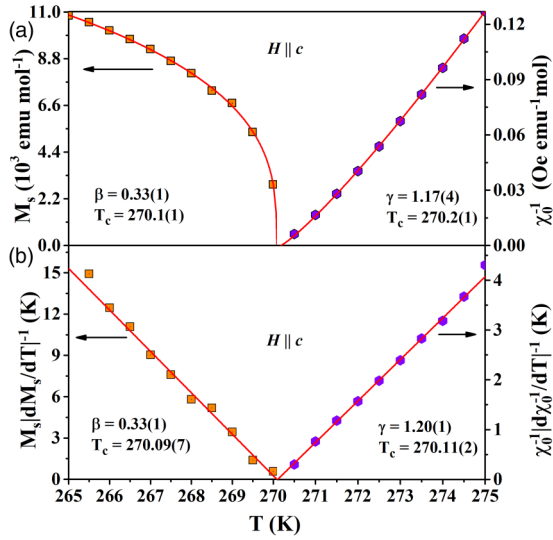


FIG. 8. (a) Temperature dependence of M_S and χ_0^{-1} for $H\parallel c$ along with the power-law fits (solid lines) following Eqs. (1) and (2). The least-squares fitting yields the values of the exponents and T_C mentioned in the plot. (b) Kouvel-Fisher plot of M_S and χ_0^{-1} as mentioned in the text. The exponents and T_C are obtained from the linear fits (solid lines) of the data in this plot.

The accuracy of the derived exponents as well as T_C was further checked using the Kouvel-Fisher technique [25]. According to this method $M_S(dM_S/dT)^{-1}$ vs T and $\chi_0^{-1}(d\chi_0^{-1}/dT)$ vs T should be straight lines with slopes $1/\beta$ and $1/\gamma$, respectively, and their intercepts on the T axis give the value of T_C . The linear fits to these plots [shown in Figs. 7(b) and 8(b)] yield $\beta = 0.376(19)$ with $T_C = 270.2(2)$ and $\gamma = 1.20(5)$ with $T_C = 270.1(3)$ for $H\parallel ab$ and $\beta = 0.33(1)$ with $T_C = 270.09(7)$ and $\gamma = 1.20(12)$ with $T_C = 270.11(2)$ for $H\parallel c$.

Using the values of critical exponents β and γ obtained from the modified Arrott plots and the Kouvel-Fisher plots, the values of the corresponding critical exponent δ are estimated from the Widom scaling relation [26]

$$\delta = 1 + \frac{\gamma}{\beta} \quad (7)$$

and are compiled in Table I. To check that the estimated values of β , γ , and T_C of Fe_4GeTe_2 also obey the scaling theory of the equation of magnetic states given by Eq. (5), scaled m vs scaled h is plotted on a log-log scale using the values of critical exponents β , γ , and T_C obtained from the modified Arrott plots in Figs. 6(a) and 6(b) for $H\parallel ab$ and for $H\parallel c$, respectively. Figure 9 shows that all the isotherms above T_C collapse onto the single curve f_+ , whereas all the isotherms below T_C collapse onto the single curve f_- for both $H\parallel ab$ and $H\parallel c$ orientations of the applied magnetic field. The critical exponent δ can also be estimated from the critical isotherm following Eq. (3). According to Eq. (3), a log-log plot of the critical isotherm should yield a straight line with a slope of $1/\delta$. The insets of Figs. 9(a) and 9(b) show the critical isotherms on the log-log scale for $H\parallel ab$ and $H\parallel c$, respectively. Linear fits to the corresponding data yield $\delta = 4.21(1)$ for $H\parallel ab$ and $\delta = 4.52(1)$ for $H\parallel c$. These values

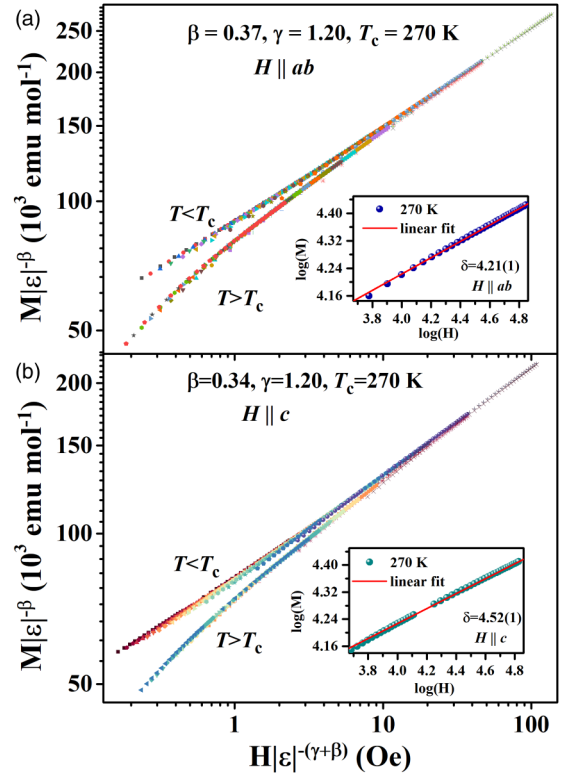


FIG. 9. (a) The log-log plot of the scaled magnetization m and the scaled field h above and below T_C for Fe_4GeTe_2 . The inset shows the field dependence of the magnetization isotherm at $T_C = 270.0$ K for Fe_4GeTe_2 plotted in log-log scale, where the solid line is the linear fit following Eq. (3) that gives the critical exponent δ mentioned in the graph. (b) The corresponding plots with the estimated value of the critical exponent δ for isotherms measured with magnetic field parallel to the c axis of the Fe_4GeTe_2 single crystal.

of the critical exponent δ are in good agreement with that obtained from Widom's scaling relation (Table I). Therefore, the obtained values of critical exponents and T_C for the Fe_4GeTe_2 compound are self-consistent and obey the scaling hypothesis.

The critical exponents and the critical temperature estimated using the above-mentioned techniques for the Fe_4GeTe_2 single crystal are tabulated and compared with several other related systems as well as with the values predicted for different theoretical models in Table I. From Table I, it can be seen that the estimated critical exponents for Fe_4GeTe_2 do not completely belong to any conventional universality class for the 3D system but fall between values predicted by the 3D Heisenberg model and the mean-field theory. The reduced temperature range used to derive the critical exponents for Fe_4GeTe_2 is $7.4 \times 10^{-4} \leq \varepsilon \leq 2.2 \times 10^{-2}$, which falls well inside the asymptotic critical regime, equal to $|\varepsilon| \simeq 10^{-2}$ for homogeneous magnets. Therefore, the observed discrepancy from the 3D Heisenberg values may result from two possibilities: (i) exchange interaction of extended type, i.e., interaction beyond the nearest neighbor, and (ii) magnetic inhomogeneity in the system. The presence of the extended type of magnetic exchange has been shown in some other members of the Fe_nGeTe_2 family [27–29]. The extended type of interaction can arise from isotropic exchange interaction

between spins involving itinerant electrons that decay spatially as $J(r) = 1/r^{d+\sigma}$, where d is the effective dimensionality of the spin interaction and σ is a measure of the range of the exchange interaction [32]. In 3D isotropic magnets with $\sigma > 2$, the 3D Heisenberg model is realized, where $J(r)$ decreases with r faster than r^{-5} due to short-range magnetic exchange. Mean-field exponents are realized when $J(r)$ decreases slower than $r^{-4.5}$. For $3/2 \leq \sigma \leq 2$, the system belongs to a different class with critical exponents that take intermediate values depending on σ . A renormalization group theory analysis predicts the susceptibility exponent γ as follows:

$$\gamma = 1 + \frac{4}{d} \left(\frac{n+2}{n+8} \right) \Delta\sigma + \frac{8(n+2)(n-4)}{d^2(n+8)^2} \times \left\{ 1 + \frac{2G(\frac{d}{2})(7n+20)}{(n-4)(n+8)} \right\} \Delta\sigma^2, \quad (8)$$

where $\Delta\sigma = (\sigma - \frac{d}{2})$ and $G(\frac{d}{2}) = 3 - \frac{1}{4}(\frac{d}{2})^2$. d and n are the dimensionality of lattice and spin, respectively. Using Eq. (8) together with different scaling relations predicted by the scaling hypothesis such as $\alpha = 2 - \nu d$, $\beta = (2 - \alpha - \gamma)$, and $\delta = 1 + \gamma/\beta$, the values of d , n , and σ , which yield values of critical exponents close to that found experimentally for Fe_4GeTe_2 , can be calculated. To do so, the value of σ is initially adjusted in Eq. (8) for several sets of $\{d : n\}$ to obtain a proper value of γ that matches well with the experimental value of $\gamma = 1.20$. The obtained σ is then used to calculate other critical exponents from the scaling relations mentioned before. The calculated critical exponents for several sets of $d:n$ and proper σ values are compiled in Table I. From the Table I we can see that for $\{d : n\} = 3 : 3$, the calculated value of the critical exponent $\beta = 0.423$, which is significantly larger than the experimental value of β but matches quite well for $\{d : n\} = 2 : 1$. However, $n = 1$ or Ising spin is not feasible as magnetism in Fe_4GeTe_2 appears to be quite isotropic [Figs. 2(b) and 3] and the small magnetic anisotropy, together with the high T_C , in Fe_4GeTe_2 is clearly off from the trend of any Ising systems [13]. This indicates that the effective dimensionality of the magnetic network in Fe_4GeTe_2 is less than 3D. Thus, the magnetism in Fe_4GeTe_2 is quasi-2D in nature and the exchange interaction is the long-range type that decreases spatially slower than $r^{-4.76}$, consistent with the quasi-two-dimensional ferromagnetic behavior observed from the analysis based on the self-consistent renormalization (SCR) theory of spin fluctuations as described below.

To shed some light on the nature of ferromagnetism in the Fe_4GeTe_2 single crystal, the magnetization isotherm at T_C has been analyzed based on Takahashi's self-consistent renormalization theory for itinerant systems in which the conservation of zero-point spin fluctuations and thermal spin fluctuations is considered [33–35].

According to the SCR theory, the magnetization M at T_C should obey the following relation:

$$M^4 = \frac{1}{4.671} \left(\frac{T_C^2}{T_A^3} \right) \left(\frac{H}{M} \right), \quad (9)$$

where M and H are in units of $\mu_B/\text{mol Fe}$ and Oe, respectively. T_A (in K) is the dispersion of the spin fluctuation

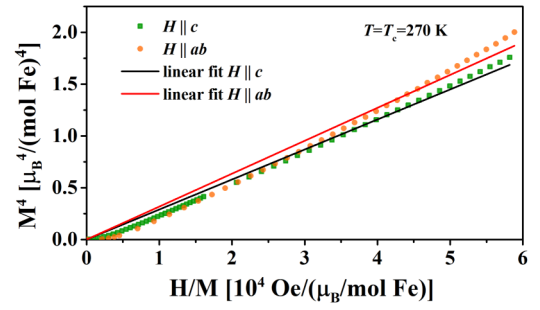


FIG. 10. M^4 vs H/M plot for the Fe_4GeTe_2 single crystal at $T = T_C = 270$ K for both the $H \parallel ab$ and $H \parallel c$ orientations of the applied magnetic field.

spectrum in wave-vector space. Such a linear behavior of magnetization [Eq. (9)] at T_C has been observed in many itinerant ferromagnetic compounds such as Fe_3GeTe_2 , LaCo_2P_2 , $\text{FeGa}_{3-y}\text{Ge}_y$, SmCoAsO , and MnSi [36–40]. Figure 10 shows the M^4 vs H/M plot of the critical magnetization isotherm for applied field parallel to the ab plane and c axis of the Fe_4GeTe_2 single crystal. The data were fitted using Eq. (9), and the linear fits yield the values of the slope of $2.89(2) \times 10^{-5} [\mu_B/(\text{mol Fe})]^5/\text{Oe}$ for $H \parallel c$ and $3.18(3) \times 10^{-5} [\mu_B/(\text{mol Fe})]^5/\text{Oe}$ for $H \parallel ab$. Using these slopes and $T_C = 270$ K for Fe_4GeTe_2 , we obtain $T_A = 813.7$ and 789.0 K for $H \parallel c$ and $H \parallel ab$, respectively. The SCR theory further predicts that T_C of the system is governed by

$$T_C = (60c)^{-3/4} P_S^{3/2} T_A^{3/4} T_0^{1/4}, \quad (10)$$

where $c = 0.3353$, P_S is the spontaneous magnetization in Bohr magneton, and T_0 is the energy width of the dynamical spin fluctuation spectrum. Using the values of T_C , P_S , and T_A estimated above, we obtain the characteristic temperature $T_0 = 1707.3$ K for Fe_4GeTe_2 . Since the best linear fit to Eq. (9) is obtained for $H \parallel c$, the corresponding T_A value is used in the estimation of the spin fluctuation parameter T_0 . According to the SCR theory of spin fluctuations, the ratio T_C/T_0 is an important parameter as it characterizes the degree of localization or itineracy of the spin moment [35]. For $T_C/T_0 \ll 1$, magnetic materials have a strong itinerant character, while for $T_C/T_0 \sim 1$, they exhibit local moment magnetism. For Fe_4GeTe_2 , T_C/T_0 is estimated to be 0.16, which is much smaller than 1 and comparable to the values reported for weak ferromagnets, such as MnSi (0.13), $\text{Fe}_{0.77}\text{Co}_{0.23}\text{Si}$ (0.1), and Fe_3GeTe_2 (0.096) [35,36].

The nature of magnetism revealed by the SCR theory can be checked further using the value of the Rhodes-Wohlfarth ratio (RWR), which is defined as P_C/P_S , where $P_C(P_C + 2) = P_{\text{eff}}^2$ and P_S is the saturation magnetization. Using the values of P_{eff} [Fig. 2(b)] and P_S (Fig. 3), the estimated values of RWR of the Fe_4GeTe compound are 2.53 for $H \parallel ab$ and 2.48 for $H \parallel c$. These values are larger than 1, indicating that the local moment description of magnetism is inadequate for the ferromagnetic Fe_4GeTe_2 single crystal. The RWR for Fe_4GeTe_2 is found to be smaller than the value reported for Fe_3GeTe_2 (RWR = 3.8), which indicates that the itinerant character of the Fe_nGeTe_2 system is suppressed with the increase in Fe concentration [29,36]. On the

basis of the SCR theory of spin fluctuations, a generalized Rhodes-Wohlfarth ratio is given as $P_{\text{eff}}/P_S \sim 1.4(T_C/T_0)^{-2/\beta}$. A value of $P_{\text{eff}}/P_S = 2.963$ is obtained for Fe_4GeTe_2 , which is slightly smaller than the generalized Rhodes-Wohlfarth value of ~ 4.78 . This could be attributed to the reduced dimensionality ($d < 3$) of Fe_4GeTe_2 , where a smaller P_{eff}/P_S results as the dimensionality decreases from 3D to 2D for the same T_C/T_0 [41]. This seems to be consistent with the renormalization group theory analysis of the critical exponent for Fe_4GeTe_2 (Table I), where the value of the critical exponent β suggests a reduced dimensionality from 3D. Therefore, a quasi-2D ferromagnetism, intermediate between the localized and itinerant systems, is anticipated in the Fe_4GeTe_2 compound.

A comprehensive study of critical exponents values for 2D magnets proposed that the critical exponent β should lie in the window of $0.1 \leq \beta \leq 0.25$ [42]. The critical exponent $\beta = 0.37$ obtained from the magnetization where the magnetic field was applied along the magnetic easy axis ($H \parallel ab$) and the renormalization group theory analysis based on the experimental value of the critical exponent $\gamma = 1.20$ indicate that the interlayer magnetic interaction is significant and the magnetic network of Fe atoms in the Fe_4GeTe_2 single crystal is quasi-2D in nature. Furthermore, a small reduction in the value of the critical exponent β for the magnetization measured with magnetic field applied along the c axis ($H \parallel c$) implies the presence of a weak anisotropy in the magnetic coupling in the Fe_4GeTe_2 single crystal. The effective uniaxial magnetic anisotropy K_{eff} calculated from the saturation field H_S and saturation magnetization M_S is defined as $2\frac{K_{\text{eff}}}{M_S} = H_S$. The obtained value of K_{eff} is 0.31 J/cm^3 . This appears to be consistent with the observed small value ($K_{\text{eff}} = 0.23 \text{ J/cm}^3$) from an earlier report which originates from the competition between the magnetocrystalline anisotropy and the shape anisotropy [13]. In contrast, Fe_3GeTe_2 shows a strong uniaxial magnetic anisotropy of $K_{\text{eff}} = 1.03 \text{ J/cm}^3$, which is more than 3 times larger than that for Fe_4GeTe_2 . This is also consistent with the fact that a smaller value of $\beta = 0.322$ has been reported for the Fe_3GeTe_2 single crystal (Table I). Therefore, an increase in the Fe concentration strengthens the interlayer exchange interaction in Fe_4GeTe_2 compared to Fe_3GeTe_2 . The critical behavior study of Fe_5GeTe_2 reported its critical

exponent $\beta = 0.346(10)$ and $\gamma = 1.364(9)$ (see Table I). Although the value of β for Fe_5GeTe_2 matches quite well that observed in Fe_4GeTe_2 for $H \parallel c$, the value of γ is found to be much larger than that for Fe_4GeTe_2 . Thus, it appears that Fe plays a detrimental role in the magnetic exchange and the nature of the magnetic exchange mechanism is quite complex in the quasi-two-dimensional vdW Fe_nGeTe_2 ($n \geq 3$) ferromagnets.

IV. CONCLUSION

An in-depth study of critical phenomena in the quasi-two-dimensional itinerant Fe_4GeTe_2 ferromagnet showed that the compound undergoes a continuous PM to FM phase transition at $T_C = 270.2 \text{ K}$. The values of the critical exponents suggest that the interlayer magnetic interaction is significant, and the compound exhibits a critical behavior of a quasi-2D magnet. A small reduction in the value of the critical exponent β obtained from magnetization measured with magnetic field applied parallel to the c axis confirmed the weak effective uniaxial magnetic anisotropy in the Fe_4GeTe_2 single crystal. The exponents of Fe_4GeTe_2 do not fall in any conventional universality class of homogeneous ferromagnets; however, the exponents do satisfy the scaling relations and scaling equation of magnetic states predicted by the scaling hypothesis. The SCR theory of spin fluctuations and the renormalization group theory analysis based on the critical exponent $\gamma = 1.20$ suggest quasi-2D itinerant ferromagnetism in Fe_4GeTe_2 where the magnetic exchange constant $J(r)$ is of the extended type and decreases slower than $r^{-4.765}$. The values of spin fluctuation parameters determined from the critical isotherm based on spin-fluctuation theory and the Rhodes-Wohlfarth ratio indicate that the nature of the magnetism in quasi-2D Fe_4GeTe_2 is intermediate between the localized and itinerant systems.

ACKNOWLEDGMENTS

The authors are very grateful to Dr. D. Bhattacharya for his valuable assistance during the characterization of the sample. We acknowledge and thank Dr. A. N. Pal and R. Alam for their help in characterizing the crystal. The authors also would like to thank A. Paul for his help during measurements.

-
- [1] A. K. Geim and I. V. Grigorieva, *Nature (London)* **499**, 419 (2013).
- [2] C. Gong, L. Li, Z. Li, H. Ji, A. Stern, Y. Xia, T. Cao, W. Bao, C. Wang, Y. Wang, Z. Q. Qiu, R. J. Cava, S. G. Louie, J. Xia, and X. Zhang, *Nature (London)* **546**, 265 (2017).
- [3] B. Huang, G. Clark, E. Navarro-Moratalla, D. R. Klein, R. Cheng, K. L. Seyler, D. Zhong, E. Schmidgall, M. A. McGuire, D. H. Cobden, W. Yao, D. Xiao, P. Jarillo-Herrero, and X. Xu, *Nature (London)* **546**, 270 (2017).
- [4] T. Song, X. Cai, M. W. Tu, X. Zhang, B. Huang, N. P. Wilson, K. L. Seyler, L. Zhu, T. Taniguchi, K. Watanabe, M. A. McGuire, D. H. Cobden, D. Xiao, W. Yao, and X. Xu, *Science* **360**, 1214 (2018).
- [5] D. R. Klein, D. MacNeill, J. L. Lado, D. Soriano, E. Navarro-Moratalla, K. Watanabe, T. Taniguchi, S. Manni, P. Canfield, J. Fernández-Rossier, and P. Jarillo-Herrero, *Science* **360**, 1218 (2018).
- [6] D. Zhong, K. L. Seyler, X. Y. Linpeng, R. Cheng, N. Sivadas, B. Huang, E. Schmidgall, T. Taniguchi, K. Watanabe, M. A. McGuire, W. Yao, D. Xiao, K. M. C. Fu, and X. D. Xu, *Sci. Adv.* **3**, e1603113 (2017).
- [7] N. Samarth, *Nature (London)* **546**, 216 (2017).
- [8] Y. Wang, C. Xian, J. Wang, B. Liu, L. Ling, L. Zhang, L. Cao, Z. Qu, and Y. Xiong, *Phys. Rev. B* **96**, 134428 (2017).
- [9] K. Kim, J. Seo, E. Lee, K.-T. Ko, B. S. Kim, B. G. Jang, J. M. Ok, J. Lee, Y. J. Jo, W. Kang, J. H. Shim, C. Kim, H. W. Yeom, B. I. Min, B.-J. Yang, and J. S. Kim, *Nat. Mater.* **17**, 794 (2018).

- [10] C. Tan, J. Lee, S.-G. Jung, T. Park, S. Albarakati, J. Partridge, M. R. Field, D. G. McCulloch, L. Wang, and C. Lee, *Nat. Commun.* **9**, 1554 (2018).
- [11] A. F. May, D. Ovchinnikov, Q. Zheng, R. Hermann, S. Calder, B. Huang, Z. Fei, Y. Liu, X. Xu, and M. A. McGuire, *ACS Nano* **13**, 4436 (2019).
- [12] A. F. May, C. A. Bridges, and M. A. McGuire, *Phys. Rev. Materials* **3**, 104401 (2019).
- [13] J. Seo *et al.*, *Sci. Adv.* **6**, eaay8912 (2020).
- [14] N. D. Mermin and H. Wagner, *Phys. Rev. Lett.* **17**, 1133 (1966).
- [15] G. T. Lin, H. L. Zhuang, X. Luo, B. J. Liu, F. C. Chen, J. Yan, Y. Sun, J. Zhou, W. J. Lu, P. Tong, Z. G. Sheng, Z. Qu, W. H. Song, X. B. Zhu, and Y. P. Sun, *Phys. Rev. B* **95**, 245212 (2017).
- [16] B. Liu, Y. Zou, L. Zhang, S. Zhou, Z. Wang, W. Wang, Z. Qu, and Y. Zhang, *Sci. Rep.* **6**, 33873 (2016).
- [17] Y. Liu and C. Petrovic, *Phys. Rev. B* **97**, 014420 (2018).
- [18] G. T. Lin, X. Luo, F. C. Chen, J. Yan, J. J. Gao, Y. Sun, W. Tong, P. Tong, W. J. Lu, Z. G. Sheng, W. H. Song, X. B. Zhu, and Y. P. Sun, *Appl. Phys. Lett.* **112**, 072405 (2018).
- [19] H. Zhang, R. Chen, K. Zhai, X. Chen, L. Caretta, X. Huang, R. V. Chopdekar, J. Cao, J. Sun, J. Yao, R. Birgeneau, and R. Ramesh, *Phys. Rev. B* **102**, 064417 (2020).
- [20] H. E. Stanley, *Introduction to Phase Transitions and Critical Phenomena* (Oxford University Press, New York, 1971).
- [21] A. Arrott, *Phys. Rev.* **108**, 1394 (1957).
- [22] S. K. Banerjee, *Phys. Lett.* **12**, 16 (1964).
- [23] D. C. Cronmeyer, *J. Appl. Phys.* **70**, 2911 (1991).
- [24] A. Arrott and J. Noakes, *Phys. Rev. Lett.* **19**, 786 (1967).
- [25] J. S. Kouvel and M. E. Fisher, *Phys. Rev.* **136**, A1626 (1964).
- [26] B. Widom, *J. Chem. Phys.* **43**, 3898 (1965); **41**, 1633 (1964).
- [27] Z. Li, W. Xia, H. Su, Z. Yu, Y. Fu, L. Chen, X. Wang, N. Yu, Z. Zou, and Y. Guo, *Sci. Rep.* **10**, 15345 (2020).
- [28] B. Liu, Y. Zou, S. Zhou, L. Zhang, Z. Wang, H. Li, Z. Qu, and Y. Zhang, *Sci. Rep.* **7**, 6184 (2017).
- [29] Y. Liu, V. N. Ivanovski, and C. Petrovic, *Phys. Rev. B* **96**, 144429 (2017).
- [30] M. Campostrini, M. Hasenbusch, A. Pelissetto, P. Rossi, and E. Vicari, *Phys. Rev. B* **65**, 144520 (2002).
- [31] J. C. Le Guillou and J. Zinn-Justin, *Phys. Rev. B* **21**, 3976 (1980).
- [32] M. E. Fisher, S. K. Ma, and B. G. Nickel, *Phys. Rev. Lett.* **29**, 917 (1972).
- [33] T. Moriya and Y. Takahashi, *J. Phys. Soc. Jpn.* **45**, 397 (1978).
- [34] Y. Takahashi, *J. Phys. Soc. Jpn.* **55**, 3553 (1986).
- [35] Y. Takahashi, *Spin Fluctuation Theory of Itinerant Electron Magnetism* (Springer, Berlin, 2013).
- [36] B. Chen, J. Yang, H. Wang, M. Imai, H. Ohta, C. Michioka, K. Yoshimura, and M. Fang, *J. Phys. Soc. Jpn.* **82**, 124711 (2013).
- [37] M. Imai, C. Michioka, H. Ueda, and K. Yoshimura, *Phys. Rev. B* **91**, 184414 (2015).
- [38] Y. Zhang, Y. Takahashi, M. Imai, G. Wang, M. A. Avila, T. Takabatake, C. Michioka, H. Ueda, K. Yoshimura, and J. Ma, *AIP Adv.* **8**, 101429 (2018).
- [39] H. Ohta, C. Michioka, A. Matsuo, K. Kindo, and K. Yoshimura, *Phys. Rev. B* **82**, 054421 (2010).
- [40] M. K. Chattopadhyay, P. Arora, and S. B. Roy, *J. Phys.: Condens. Matter* **21**, 296003 (2009).
- [41] Y. Takahashi, *J. Phys.: Condens. Matter* **9**, 10359 (1997).
- [42] A. Taroni, S. T. Bramwell, and P. C. W. Holdsworth, *J. Phys.: Condens. Matter* **20**, 275233 (2008).